nature catalysis

Article

https://doi.org/10.1038/s41929-024-01134-3

Paired photoelectrochemical conversion of CO_2/H_2O and glycerol at high rate

In the format provided by the authors and unedited

Table of contents

Supplementary Note 1

The photoelectrode assembly

A clarified representation of the photoelectrode assembly can be seen in **Supplementary Figure 1**. The Ni-covered Si wafer was soldered at its backside to the printed circuit board (PCB). Epoxy was used to cover the exposed metallic parts of the PCB from the front. The assembly was immersed in the electrolyte; however, the backside of the PCB is not conductive, which leaves the Ni-covered Si (in contact with the electrolyte) as the only active part of the PEC assembly. The role of the silicone holder is to press the electrode on the small o-rings which seal the contacts from the electrolyte. The thickness of the electrolyte layer between the Si surface and the plexiglass was always 2 mm, which is precisely set by the grooves created in the anode current collector (these grooves define the place of the plexiglass). In this regard, the electrode assembly consists of a photoanode (n-type Si wafer) and a deposited catalyst layer on its surface which is in contact with the electrolyte.

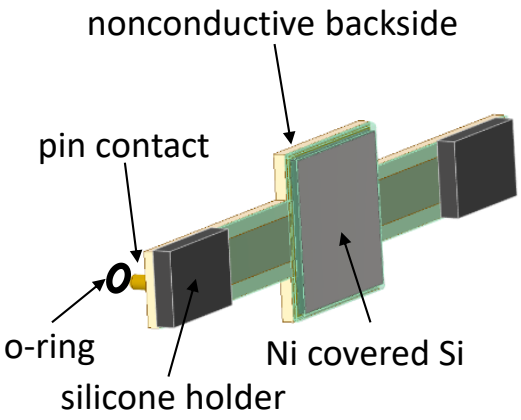

Supplementary Figure 1. Schematic representation of the used photoelectrode assembly.

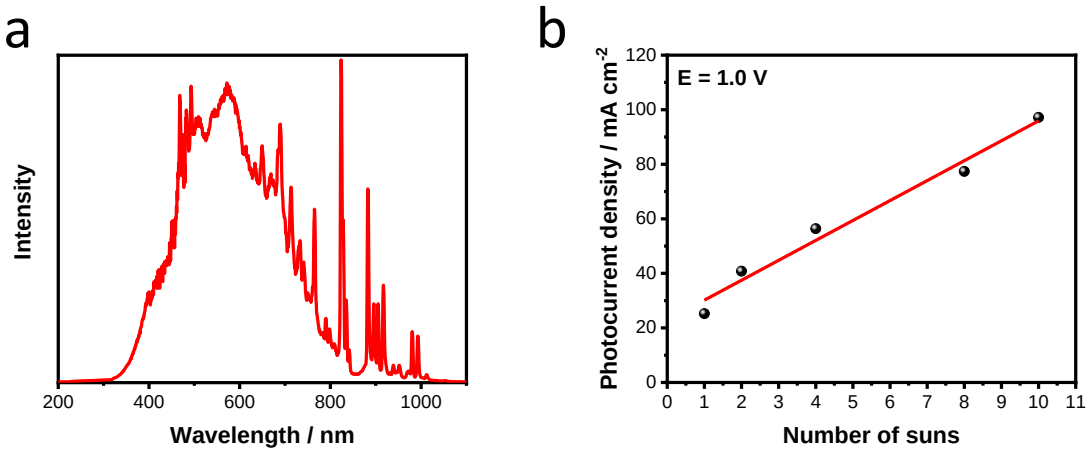

Supplementary Figure 2. (a) Spectrum of the solar simulator and (b) intensity dependence of the photocurrent derived from the photovoltammograms at 1.0 V vs. Ag/AgCl recorded in 0.5 M glycerol containing 1.0 M CsOH.

Supplementary Note 2

Calculation of the Faradaic efficiencies on the anode side

Six different glycerol oxidation products were quantified after the (photo)electrochemical reaction. Five of them were analyzed by ion chromatography (oxalate, tartronate, glycerate, glycolate, formate), and one of them was determined by NMR spectroscopy (lactate). Lactate can also be separated from the other products with the column used in the ion chromatograph, but its retention time coincides with the retention time of glycerol which makes the detection impossible.

Six-point calibration was carried out for all products by using the same matrix in all cases which was 0.5 M glycerol containing 1 M CsOH (this corresponds to the composition of the real samples). After performing the electrochemical experiments, the concentration of different products was determined in the anolyte. Knowing the volume of the recirculated electrolyte (40 cm^3), the moles formed of the given product (n) were calculated. Using the total charge passed during the electrochemical measurement (Q), the Faraday constant (F) and the number of electrons required to form 1 mol of the given product (z), the Faradaic efficiencies (FEs) were calculated for each product using **Supplementary Equation 1**.

$$FE(\%) = \frac{n \cdot z \cdot F}{Q} \cdot 100\% \quad (1)$$

The number of electrons used in the calculations of the FEs to produce the given glycerol oxidation product is summarized in **Supplementary Table 1**.

Supplementary Table 1: Number of electrons used in the calculations of the FEs for each glycerol oxidation products.

Glycerol oxidation product	**Number of electrons to form 1 mol of the given product**
oxalate	22/3
tartronate	8
glycerate	4
glycolate	10/3
formate	8/3
lactate	2

Calculation of the Faradaic efficiencies on the cathode side

The calibration of the gas chromatograph was performed with a H_2, CO, CH_4 and C_2H_5 containing gas mixture in the range of 0.1 and 10 V/V%.

During the gas product analysis, the gas outlet on the cathode side was connected to the gas chromatograph and the sample portions were injected to the column by an automatized 6-port valve from the continuously flowing gas mixture (which contained CO_2, CO and H_2 in the case of the CO_2RR experiments). Two important parameters were registered at the exact moment of the injection: the total current density and the volumetric flow rate of the gas mixture.

The FEs of the gas products were calculated using **Supplementary Equation 2** and **3**.

$$I_i = \frac{V_i}{V_m} \cdot f \cdot z_i \cdot F \quad (2)$$

$$FE(\%) = \frac{I_i}{I_{total}} \cdot 100\% \quad (3)$$

I_i: partial current density of the given product;

V_i: volume concentration of the given product obtained from a previous calibration of the gas chromatograph;

V_m: molar volume at 1 atm and at 298.15 K

f: volumetric flow rate of the gas mixture leaving the cathode compartment of the cell at the time of injection into the gas chromatograph;

z_i: number of transferred electrons to form 1 mol of the given product (z_i=2 both for H_2 and CO);

F: Faraday constant (96485 C mol^{-1});

I_{total}: total current density measured during (photo)electrolysis at the time of injection into the gas chromatograph.

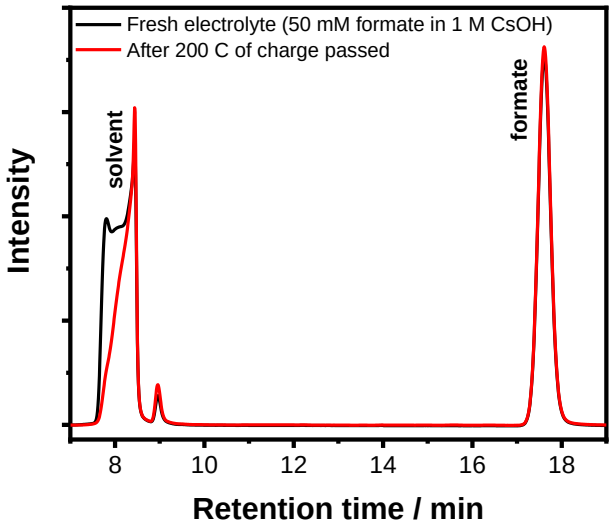

Supplementary Figure 3. Ion chromatograms at 200 nm of 50 mM formate containing 1 M CsOH before and after the galvanostatic PEC experiment at 50 mA cm^{-2} for 4000 s (200 C of charge passed) under 10 sun irradiation.

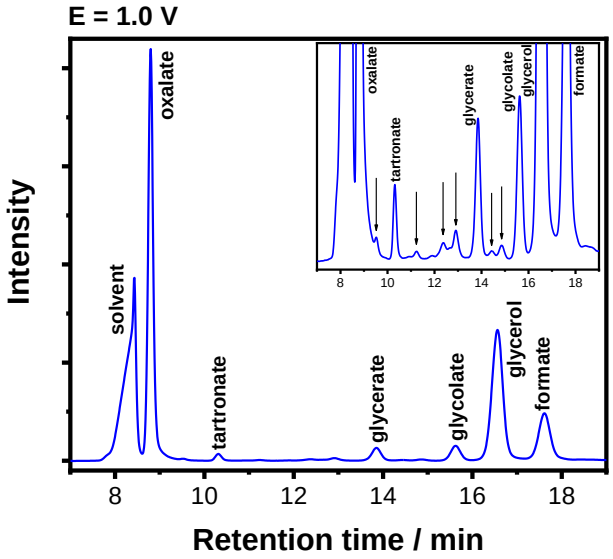

Supplementary Figure 4. Ion chromatogram at 200 nm which shows the peak of the remaining glycerol and the peaks of the main products after the PEC reaction at 1.0 V vs. Ag/AgCl. The black arrows on the inset indicate the byproducts from the spontaneous decomposition of the intermediates.

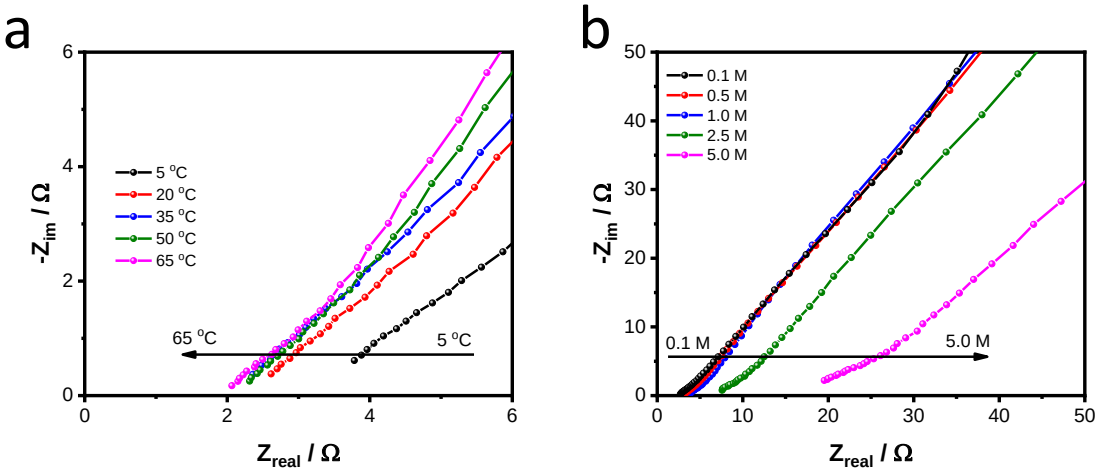

Supplementary Figure 5. Electrochemical impedance spectroscopic measurements between the anode and the cathode at open circuit voltage. The measurements were performed (a) at different temperatures and (b) at different concentrations of glycerol. The anolyte flow rate was 10 cm^3 min^{-1}, while the argon stream was set to 25 cm^3 min^{-1}.

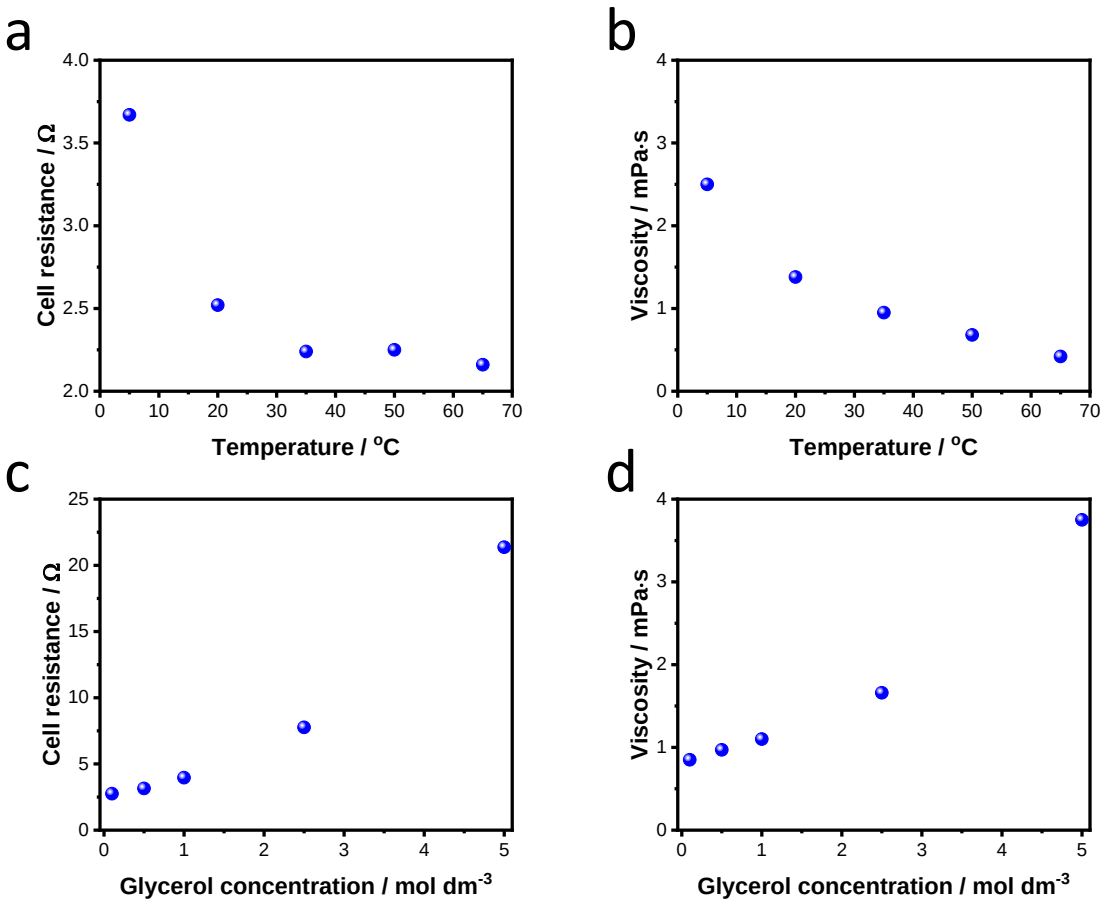

Supplementary Figure 6. Effect of temperature (a,b) and glycerol concentration (c,d) on the cell resistance (a,c) and anolyte viscosity (b,d). The cell resistance values derived from the Nyquist plots (shown in **Supplementary Figure 5**).

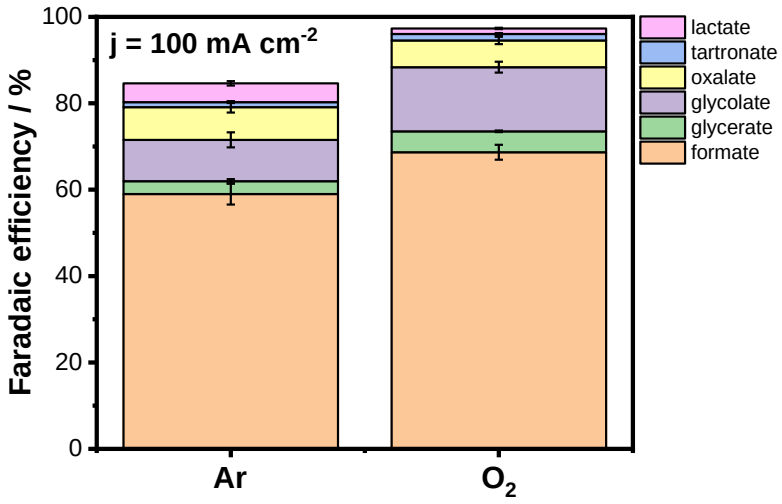

Supplementary Figure 7. Product distribution using argon deaerated and oxygen saturated anolyte after 30 minutes galvanostatic experiments at 100 mA cm^{-2} current densities under 1000 mW cm^{-2} light intensity (10 sun). The anolyte was 0.5 M glycerol containing 1.0 M CsOH. HER was performed on the cathode side using 25 cm^3 min^{-1} argon flow, while the anolyte flow rate was 10 cm^3 min^{-1}. The temperature of the cell and the anolyte was 35 ^oC. The error bars represent the standard deviation from the average (mean), originated from three separate measurements performed on three different Ni/Si electrodes.

Supplementary Note 3

The origin of the missing Faradaic efficiency on the anode side

To visualize the color difference between the argon deaerated and oxygen saturated anolyte after the PEC oxidation of glycerol, UV-Vis absorbance spectra were measured for these solutions (**Supplementary Figure 8a**). In the case of the argon deaerated electrolyte, an additional broad absorbance was observed in the near ultraviolet region together with a shoulder in the visible regime (red curve in **Supplementary Figure 8a**). These absorbance features were not detected in the oxygen saturated solution (black curve in **Supplementary Figure 8a**). The absorbance spectrum of the argon deaerated solution, however, changed over time (**Supplementary Figure 8b**) in parallel with the disappearance of the yellowish color when the electrolyte was exposed to air (or oxygen). In order to assign the additional absorbance to specific products, first we measured the absorbance spectra of dihydroxyacetone (**Supplementary Figure 9a**) and glyceraldehyde (**Supplementary Figure 9b**) containing anolyte. Both products have yellowish color in the anolyte which appears as an absorbance shoulder in the visible region. In addition, both products give an absorption peak in the UV region. Moreover, both intermediates showed the same behavior over time as the argon deaerated sample, namely (i) the absorbance maximum in the UV region decreased and shifted to lower wavelengths, (ii) the absorbance shoulder in the visible regime (i.e. the yellow color) disappeared (**Supplementary Figure 9a and 9b**). The broad absorbance spectrum of the argon deaerated sample (red curve in **Supplementary Figure 8a and 8b**) indicates, however, that both of the mentioned intermediates are present together, which is not surprising since they are in equilibrium. Because of this, the two intermediate products were mixed in a 1:1 ratio into the anolyte, then the absorbance spectrum of this mixture was measured over time (**Supplementary Figure 8c**). Both the initial spectrum and its change were the same as those experienced with the argon deaerated sample. Based on these observations, the unaccounted ~15% Faradaic efficiency in the case of argon deaerated sample comes from dihydroxyacetone, glyceraldehyde and oxygen but the quantification of these products is not possible as their amount continuously changes.

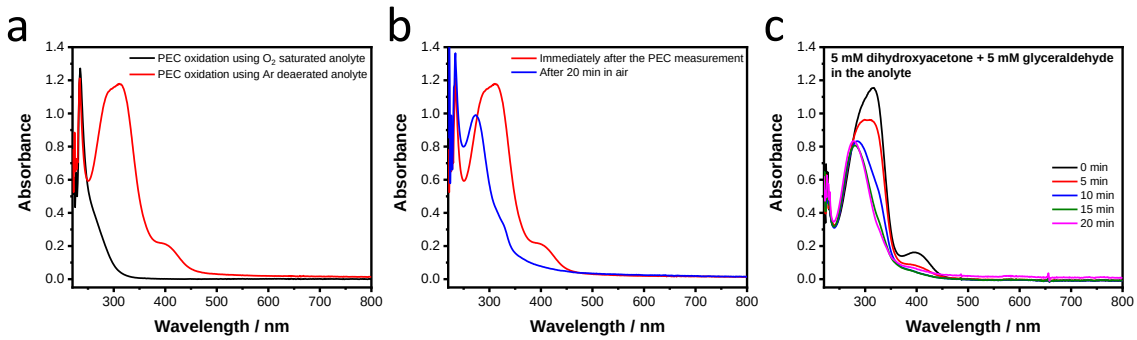

Supplementary Figure 8. (a) UV-Vis absorbance spectra of oxygen saturated anolyte (black curve) and argon deaerated anolyte (red curve) after PEC oxidation of glycerol at 100 mA cm^{-2} for 30 min. (b) UV-Vis absorbance spectra of argon deaerated sample immediately after the PEC experiment (red curve) and after 20 minutes (blue curve). (c) UV-Vis absorbance spectrum of 5 mM dihydroxyacetone and 5 mM glyceraldehyde and its change over time. The blank spectrum was recorded for fresh anolyte (0.5 M glycerol containing 1 M CsOH).

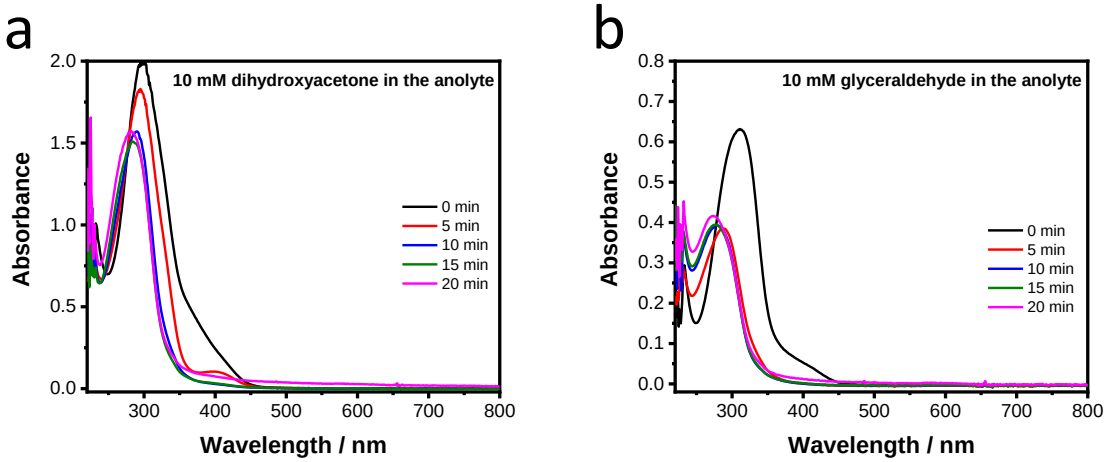

Supplementary Figure 9. UV-Vis absorbance spectra of (a) 10 mM dihydroxyacetone and (b) 10 mM glyceraldehyde and their change over time. The blank spectrum was recorded for fresh anolyte (0.5 M glycerol containing 1 M CsOH).

Supplementary Note 4

Effect of irradiation intensity on the product distribution

To examine the effect of irradiation intensity on the product distribution, potentiostatic measurements were performed at 0.6 and 1.0 V (vs. Ag/AgCl) for 30 minutes both under 1 and 10 sun (**Supplementary Figure 10a**). Beside the higher current densities that can be achieved with 10 sun, there is also a slight difference in the product distribution (**Supplementary Figure 10b and 10c**). The total FE belonging to stable products is higher under 1 sun both at 0.6 and 1.0 V (vs. Ag/AgCl), mainly because of the higher FE of glycolate and lactate.

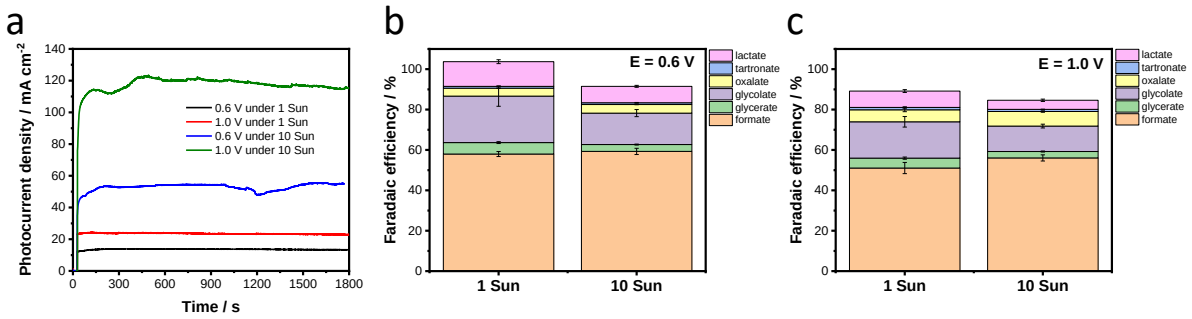

Supplementary Figure 10. Effect of irradiation intensity on the PEC oxidation of glycerol: measurements under potential control. (a) Photocurrent density over time at 0.6 and 1.0 V vs. Ag/AgCl both under 1 and 10 sun irradiation. (b,c) Product distribution in the anolyte after 30 minutes potentiostatic experiment under 1 and 10 sun (b) at 0.6 V and (c) at 1.0 V. The anolyte was 0.5 M glycerol containing 1.0 M CsOH. HER was performed on the cathode side using 25 cm^3 min^{-1} argon flow, while the anolyte flow rate was 10 cm^3 min^{-1}. The temperature of the cell and the anolyte was 35 ^oC. The error bars represent the standard deviation from the average (mean), originated from three separate measurements performed on three different Ni/Si electrodes.

To prove that the slightly different product distribution under potential control is caused by the different reaction rate, galvanostatic experiments were carried out under 1 and 10 sun at the same (25 mA cm^{-2}) current density (**Supplementary Figure 11**). As expected from **Figure 3b**, lower anode potential is required to maintain the same current density under concentrated sunlight (**Supplementary Figure 11a**). More importantly, the product distribution is independent on the irradiation intensity when the reaction rate is the same (**Supplementary Figure 11b**). Based on these measurements, the product distribution depends on the current density and not on the anode potential.

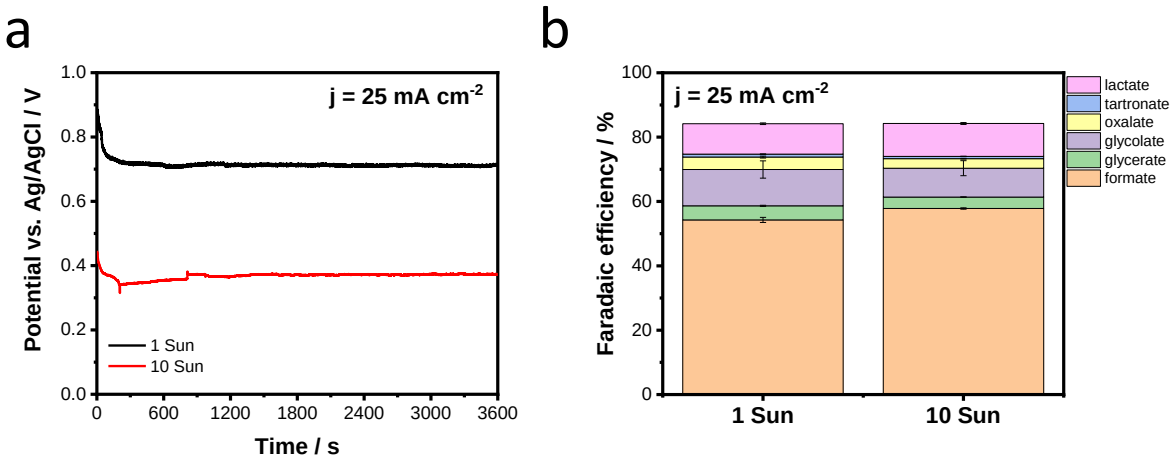

Supplementary Figure 11. Effect of irradiation intensity on the PEC oxidation of glycerol: measurements under current control. (a) Anode potential over time at 25 mA cm^{-2} current density both under 1 and 10 sun irradiation. (b) Product distribution in the anolyte after 60 minutes galvanostatic experiment at 25 mA cm^{-2} under 1 and 10 sun. The anolyte was 0.5 M glycerol containing 1.0 M CsOH. HER was performed on the cathode side using 25 cm^3 min^{-1} argon flow, while the anolyte flow rate was 10 cm^3 min^{-1}. The temperature of the cell and the anolyte was 35 ^oC. The error bars represent the standard deviation from the average (mean), originated from three separate measurements performed on three different Ni/Si electrodes.

Supplementary Table 2. Comparison of PEC and EC processes at 60 and 100 mA cm^{-2} current density. The numbers marked with red signal the potential differences on the anode side and the cell voltage differences between the anode and the cathode.

Sample	Current density / mA cm^{-2}	Anode potential / V		Cell voltage / V	
Photoelectrode	60	0.66	0.60 V	2.29	0.67 V
Dark measurement	60	1.26		2.96	
Sample	**Current density / mA cm^{-2}**	**Anode potential / V**		**Cell voltage / V**	
Photoelectrode	100	0.85	0.72 V	2.54	0.88 V
Dark measurement	100	1.57		3.42	

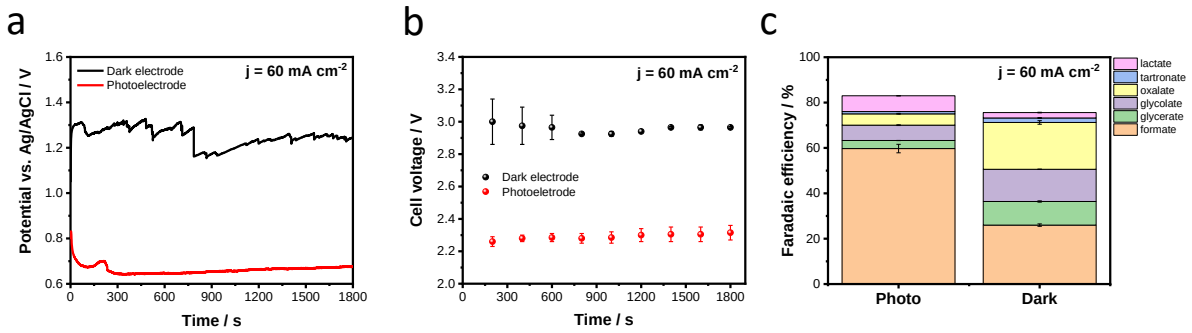

Supplementary Figure 12. Comparison of EC and PEC processes at 60 mA cm^{-2}: (a) anode potential differences during 30 minutes galvanostatic experiments, (b) cell voltage differences during 30 minutes galvanostatic experiments and (c) product distribution in the anolyte after 30 minutes galvanostatic experiments. The anolyte was 0.5 M glycerol containing 1.0 M CsOH. HER was performed on the cathode side using 25 cm^3 min^{-1} argon flow, while the anolyte flow rate was 10 cm^3 min^{-1}. The temperature of the cell and the anolyte was 35 ^oC. The error bars represent the standard deviation from the average (mean), originated from three separate measurements performed on three different Ni/Si and Ni sheet containing electrodes.

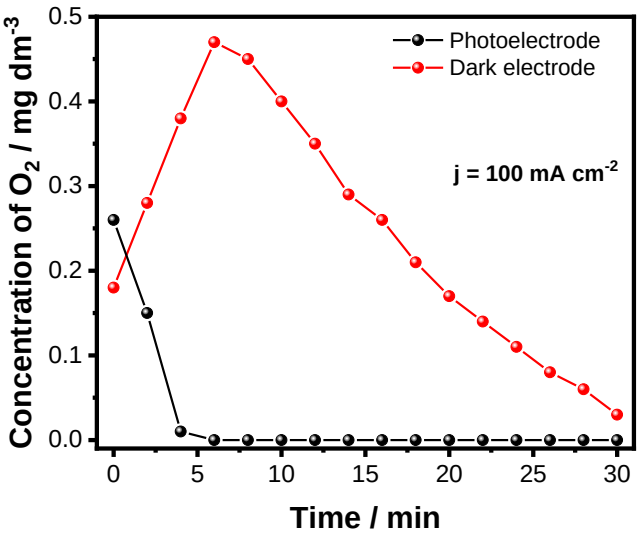

Supplementary Figure 13. Concentration of dissolved oxygen in the anolyte during 30 minutes galvanostatic EC and PEC experiments at 100 mA cm^{-2}.

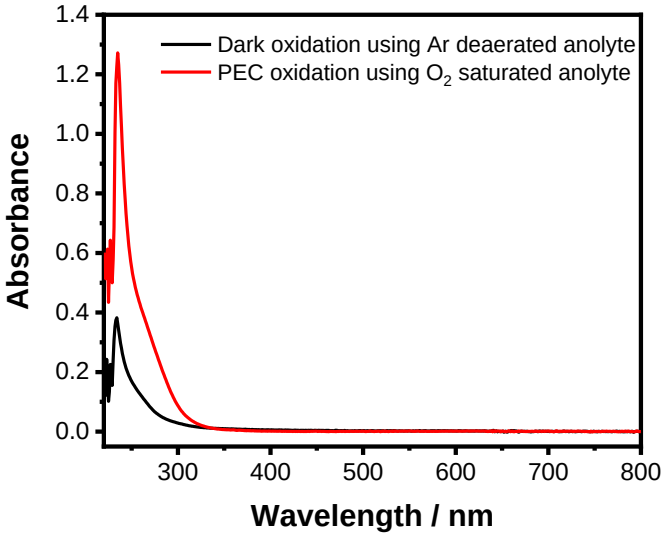

Supplementary Figure 14. UV-Vis absorbance spectra of argon deaerated anolyte after the dark oxidation (black curve) and oxygen saturated anolyte after the PEC oxidation (red curve) of glycerol at 100 mA cm^{-2} for 30 min. The blank spectrum was recorded for fresh anolyte (0.5 M glycerol containing 1 M CsOH).

Supplementary Note 5

Decrease in the anolyte pH during cathodic CO_2RR

The pH of the anolyte was measured before and after the 3 h photoelectrolysis under 10 sun both at 0.6 V and 1.0 V (vs. Ag/AgCl) (**Supplementary Figure 15a and 15b**). The initial pH of the anolyte was 13.54 which decreased to 12.90 in the experiment at 0.6 V and it was 12.65 after the measurement at 1.0 V (when cathodic CO_2R occurred). Protons are generated in the anodic glycerol oxidation reaction (see **Supplementary Equation 8**), which are completely neutralized in the case of HER, by the hydroxide ions passing through the membrane. This results in a constant pH during the experiment (the pH was 13.54 before, and 13.41 after the HER experiment at 1.0 V anode potential). In the case of CO_2R at the cathode, the ion conduction is maintained by carbonate ions. In this case, the neutralization of the protons formed at the anode can only partially take place, which ultimately leads to a decrease in the anolyte pH. Under 1 sun with CO_2RR (**Supplementary Figure 15c**), the situation was the same, the pH changed from 13.48 to 11.11 in a span of 8 hours. Importantly, the pH decrease was observed only when CO_2RR was performed on the cathode. Therefore, a relatively high decrease was observed in the bulk pH of the anolyte, however, the local pH can be even more acidic during the experiments which leads to the dissolution of Ni.

Explaining the pH decrease when CO_2RR occurs on the cathode

Assuming that the ion conduction between the cathode and the anode is maintained by carbonate ions in the case of CO_2R (as confirmed by several precedent works[1–4]), for every 2 e^-, 1 CO_3^{2-} ion reaches the anolyte through the anion exchange membrane (**Supplementary Equation 4, 5 and 6**). This carbonate consumes a H^+ ion from the anolyte (**Supplementary Equation 7**), but two protons are formed (or even more precisely 2 OH^- ions are consumed) in the glycerol oxidation process (**Supplementary Equation 8**), which ultimately leads to a decrease in the anolyte pH.

Cathode reaction (CO_2 reduction to CO):

$$CO_2 + 2e^- + H_2O \rightarrow CO + 2OH^- \quad (4)$$

The forming OH^- ions on the cathode side react immediately with the continuously flowing CO_2 gas, producing carbonate:

$$2OH^- + CO_2 \rightarrow CO_3^{2-} + H_2O \quad (5)$$

The sum of these two reactions:

$$CO_2 + 2e^- \rightarrow CO + CO_3^{2-} \quad (6)$$

Ion conductance through the membrane:

$$CO_3^{2-} + H^+ \rightarrow HCO_3^- \quad (7)$$

Anode reaction (glycerol oxidation to glyceraldehyde):

$$C_3O_3H_8 \rightarrow 2e^- + C_3O_3H_6 + 2H^+ \quad (8)$$

For every $2e^-$, 1 H^+ ion remains in the anolyte which is the reason for the decreasing pH.

Explaining the unchanged pH when HER occurs on the cathode

In the case of water reduction, the ion conductance between the cathode and the anode is maintained by hydroxide ions. The two hydroxide ions formed during the HER process (**Supplementary Equation 9**) neutralize the two protons generated in the anode reaction (**Supplementary Equation 8**), therefore the pH does not change (**Supplementary Equation 10**).

Cathode reaction (H_2O reduction to H_2):

$$2H_2O + 2e^- \rightarrow H_2 + 2OH^- \quad (9)$$

Ion conductance through the membrane:

$$2OH^- + 2H^+ \rightarrow 2H_2O \quad (10)$$

Anode reaction (glycerol oxidation to glyceraldehyde):

$$C_3O_3H_8 \rightarrow 2e^- + C_3O_3H_6 + 2H^+ \quad (8)$$

Determining the amount of dissolved Ni in the anolyte

Inductively coupled plasma mass spectrometry (ICP-MS) measurements were also performed to determine the concentration of dissolved Ni in the anolyte. The Ni content of a freshly prepared anolyte was compared with the anolytes after 8 hours photoelectrolysis both with HER and CO_2RR on the cathode (**Supplementary Figure 15c**). The fresh anolyte did not contain any Ni (or at least its concentration was under the detection limit of the instrument), while the anolyte after the PEC reaction coupled with HER contained 0.573 ± 0.003 μM, and 1.959 ±

0.010 μM after the reaction performed with CO_2R. We can conclude that Ni is present in the anolyte only after the PEC process, and its concentration is much higher when CO_2R is the cathode reaction, signaling the much faster dissolution process.

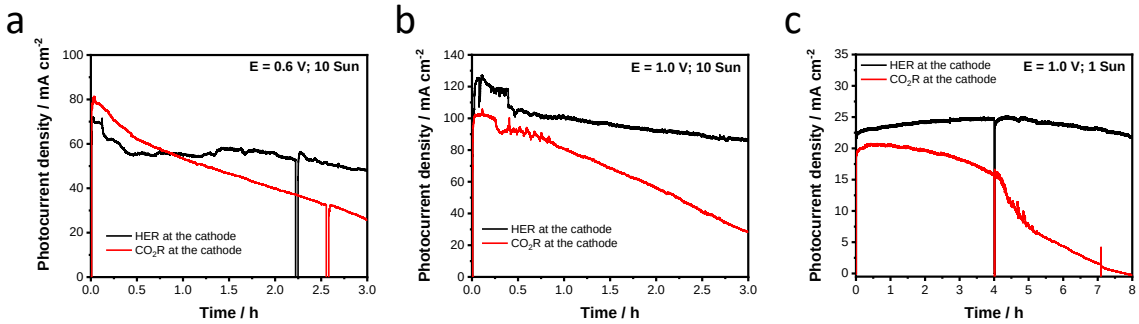

Supplementary Figure 15. Photocurrent density over time during potentiostatic experiments both with HER and CO_2RR on the cathode: (a) at 0.6 V vs. Ag/AgCl under 1000 mW cm^{-2} light intensity (10 sun), (b) at 1.0 V vs. Ag/AgCl under 1000 mW cm^{-2} light intensity (10 sun), and (c) at 1.0 V vs. Ag/AgCl under 100 mW cm^{-2} light intensity (1 sun). The anolyte was 0.5 M glycerol containing 1.0 M CsOH. HER and CO_2RR was performed on the cathode side using 25 cm^3 min^{-1} argon or CO_2 flow, while the anolyte flow rate was 10 cm^3 min^{-1}. The temperature of the cell and the anolyte was 35 ^oC.

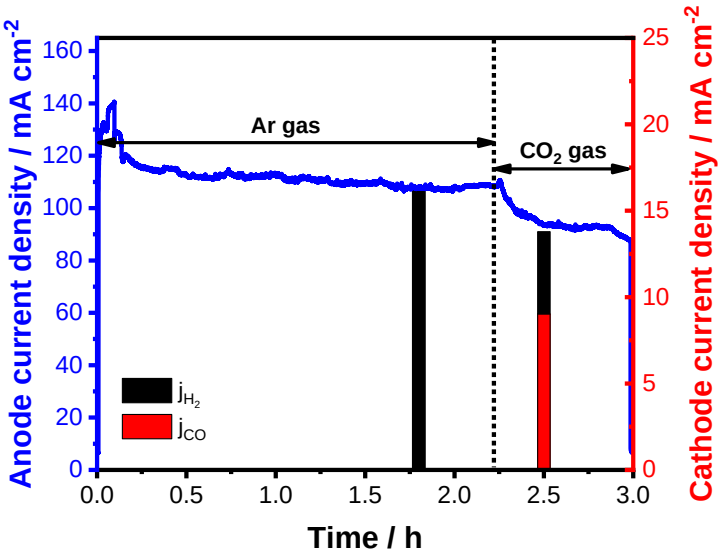

Supplementary Figure 16. Three-hour potentiostatic experiment at 1.0 V vs. Ag/AgCl operating with 1000 mW cm^{-2} light intensity (10 sun). The figure shows the photocurrent density over time together with the product distribution on the cathode side. The anolyte was 0.5 M glycerol containing 1.0 M CsOH. HER, then CO_2R was performed on the cathode side using 25 cm^3 min^{-1} argon or CO_2 flow, while the anolyte flow rate was 10 cm^3 min^{-1}. The temperature of the cell and the anolyte was 35 ^oC.

Supplementary Note 6

Anodic product distribution using PtRu catalyst

Additional potentiostatic experiments were performed at −0.3 V vs. Ag/AgCl using PtRu catalyst and the product distribution was examined after these measurements. The current densities at this potential are similar in the PEC and EC scenarios (**Figure 8a**), which can be explained by the fact that no photopotential can build up in the PtRu covered Si (as it is discussed in the manuscript, as well as in **Supplementary Figure 19**). Accordingly, there is only a slight difference in the product distribution between the EC and PEC scenarios, which is mainly due to the higher FE of lactate in the PEC process (**Supplementary Figure 17**). More importantly, the obtained products with PtRu catalyst are completely different from those determined in the case of Ni. While the amount of C3 products is negligible on Ni, the oxidation of glycerol can be performed even without C-C cleavage in the case of PtRu (the main products are glycerate, tartronate, and lactate).

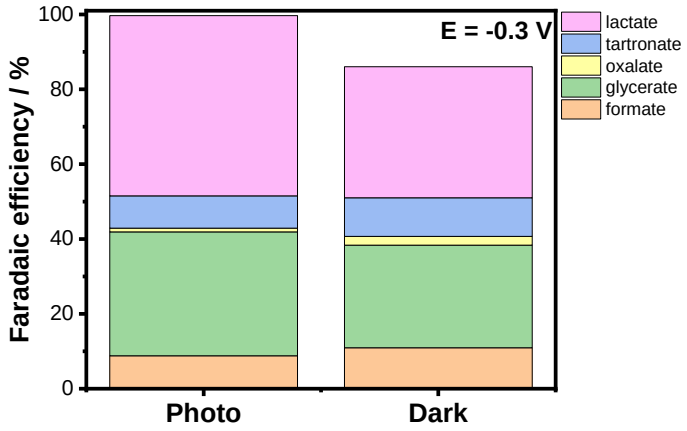

Supplementary Figure 17. Product distribution in the anolyte after PEC and EC oxidation of glycerol at -0.3 vs. Ag/AgCl anode potential using PtRu catalyst. The anolyte was 0.5 M glycerol containing 1.0 M CsOH. The PEC experiment was performed using a solar simulator (AM 1.5) as the light source operated at 1000 mW cm^{-2} (10 sun).

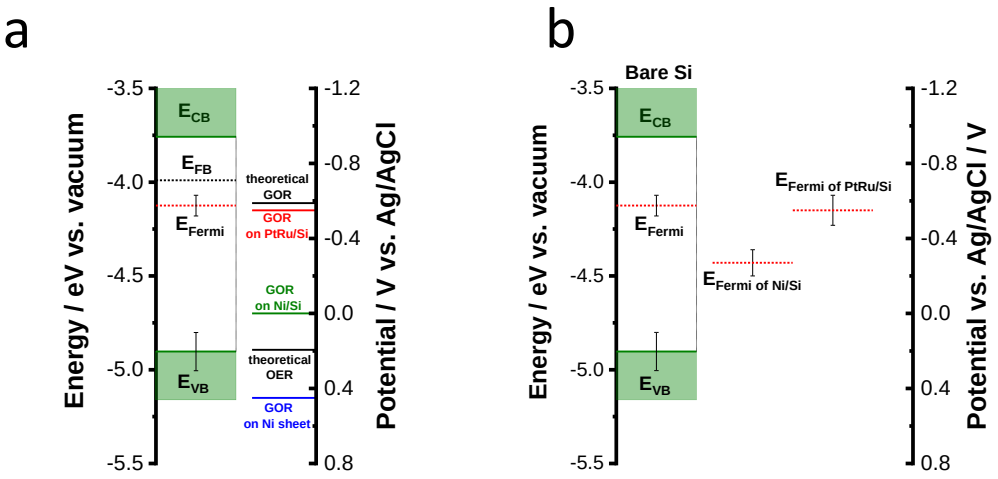

Supplementary Figure 18. (a) Band diagram of n-type Si photoanode. The VB position and the Fermi level was determined by Kelvin probe microscopy and ultraviolet photoelectron spectroscopy (UPS), while the flatband potential was identified by Mott Schottky analysis. The CB position was calculated using the optical bandgap value (1.14 eV) obtained from Tauc analysis. The theoretical onset potentials of GOR, OER and the experimentally determined onset potentials of EC and PEC GOR are also marked on the band diagram both on PtRu and Ni. (b) The position of the Fermi level before and after depositing Ni and PtRu catalysts on the surface of Si. The error bars of the VB position and the Fermi levels represent the deviation from the average (mean) value obtained by the two different methods (Kelvin probe and UPS).

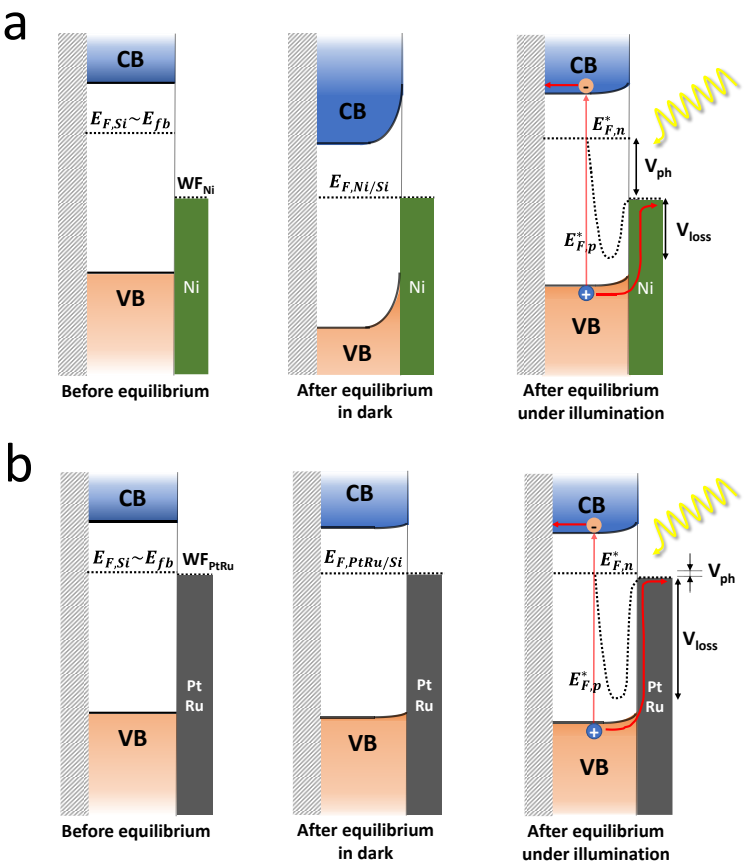

Supplementary Figure 19. Schematic energy band diagrams at the interface of (a) Ni and (b) PtRu covered n-Si photoanodes before the equilibrium, after reaching the thermodynamic equilibrium in dark and the illuminated state showing the electron-hole pair generation, separation and the developing photopotential. $E^*_{F,n}$ and $E^*_{F,p}$ represents the quasi-Fermi levels of electrons and holes, while the difference between them shows the measurable photopotential (V_{ph}).

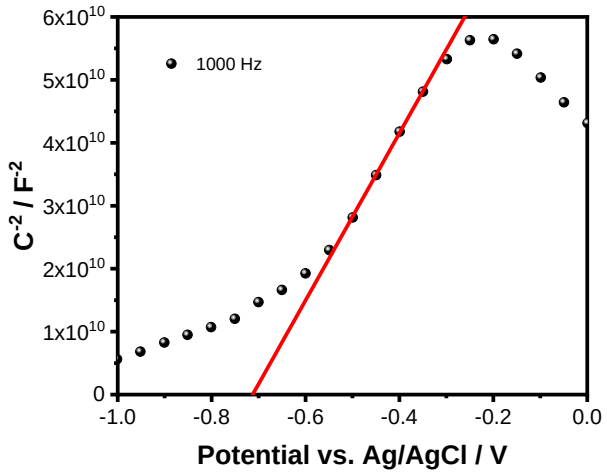

Supplementary Figure 20. Mott–Schottky plot of Ni-covered Si photoanode at 1 kHz frequency recorded in 0.5 M glycerol containing 1.0 M CsOH.

Supplementary Note 7

Operation at higher total current

In the previously described experiments, we demonstrated an efficient and stable photoanode with which industrially relevant photocurrent density and enhanced selectivity was obtained. At the same time, the geometrical surface of this photoelectrode was 1 cm^2 which means that the total current was equal to the current density. To move one step closer to the application, the surface of the photoelectrode was increased to 6.25 cm^2 which is the largest size that can still be inserted into the PEC cell shown in **Figure 1**. In these experiments, the focusing lens could not be used as its application also reduces the area of irradiation and that would not have been enough to illuminate the whole surface of the larger photoelectrode. Because of this, the light intensity was decreased from 1000 to 400 mW cm^{-2}.

Photovoltammograms were recorded to compare the photocurrent densities of the two electrodes with different surface areas (**Supplementary Figure 21**). The achievable maximum photocurrent density decreased by 30% with the sixfold increase of the electrode (39.7 mA cm^{-2} vs. 56.4 mA cm^{-2} at 1.0 V vs. Ag/AgCl). This signals that the scale up either: (i) makes the contact preparation more difficult (imperfect contact) or that (ii) the extraction of the light generated charge carriers becomes sluggish because of the longer lateral transport.

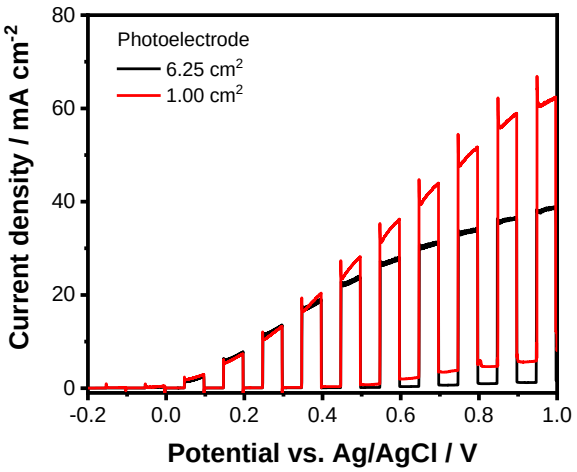

Supplementary Figure 21. Photovoltammograms of Ni-covered Si photoanodes on 6.25 and 1.00 cm^2 electrode surface. The anolyte was 0.5 M glycerol containing 1.0 M CsOH and HER was performed on the cathode side. The sweep rate was kept at 10 mV s^{-1}, while the flow rate of the anolyte was 10 cm^3 min^{-1} and 25 cm^3 min^{-1} argon stream was used on the cathode side. The experiments were performed using a solar simulator (AM 1.5) as the light source operated at 400 mW cm^{-2} (4 sun), while the light chopping frequency was 0.2 Hz. The temperature of the cell and the anolyte was 35 ^oC.

Supplementary Note 8

Characterization of the Ni-covered Si photoanode

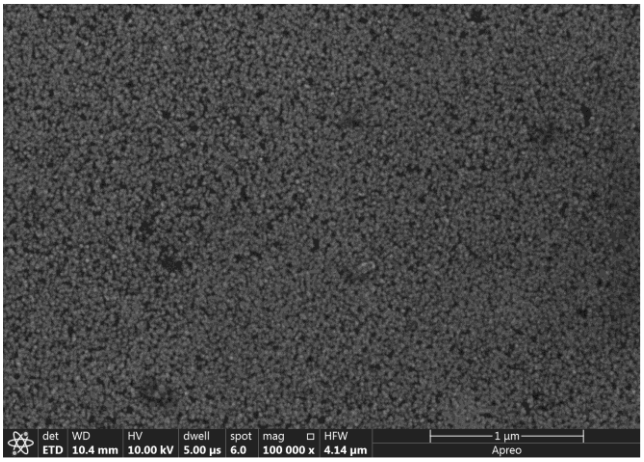

Supplementary Figure 22. SEM image of the deposited Ni catalyst on the Si wafer.

To determine the thickness of Ni layer on the Si photoabsorber, the catalyst was deposited on the half of the Si electrode, and the height of the film was measured via the edge of Ni layer on the Si substrate. Three AFM images were acquired on three different spots, and the height analysis was performed at five different regions of each image resulted a thickness of 40 ± 3 nm. The attached figure shows a representative AFM image of a selected point acquired at Ni/Si edge (**Supplementary Figure 23a**), and a vertical profile of the Ni film thickness from the region highlighted by the dashed white line (**Supplementary Figure 23b**).

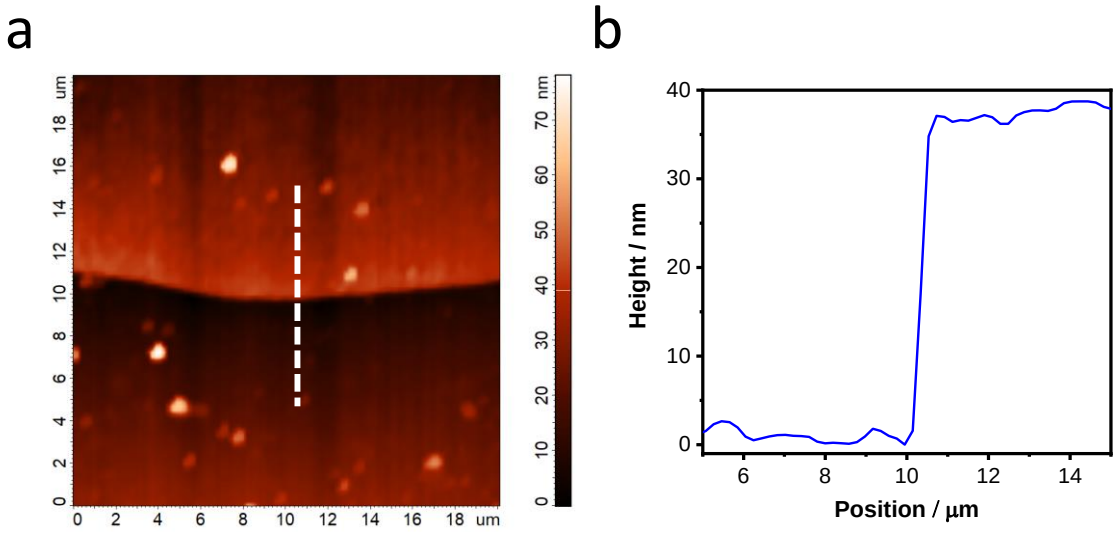

Supplementary Figure 23. (A) Representative AFM image of a selected point acquired at Ni/Si border, (B) the vertical profile of the Ni film thickness from the region highlighted by the dashed white line resulting a thickness of 40 ± 3 nm.

To assess the parasitic light absorption/reflection of the catalyst layer, transmittance spectra were measured after depositing Ni on FTO electrodes (**Supplementary Figure 24**). In this way, the amount of light that reaches the Si electrode through the Ni catalyst was quantified. There was a ~20% loss of the incident light caused by the light absorption/reflection of the catalyst layer.

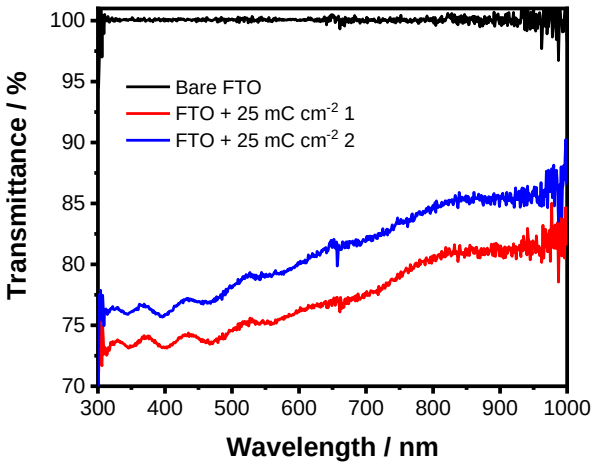

Supplementary Figure 24. Transmittance spectra of FTO electrodes before and after deposition of 25 mC cm^{-2} Ni. Red and blue curves represent two different electrodes prepared in the same way to show the reproducibility of the catalyst deposition.

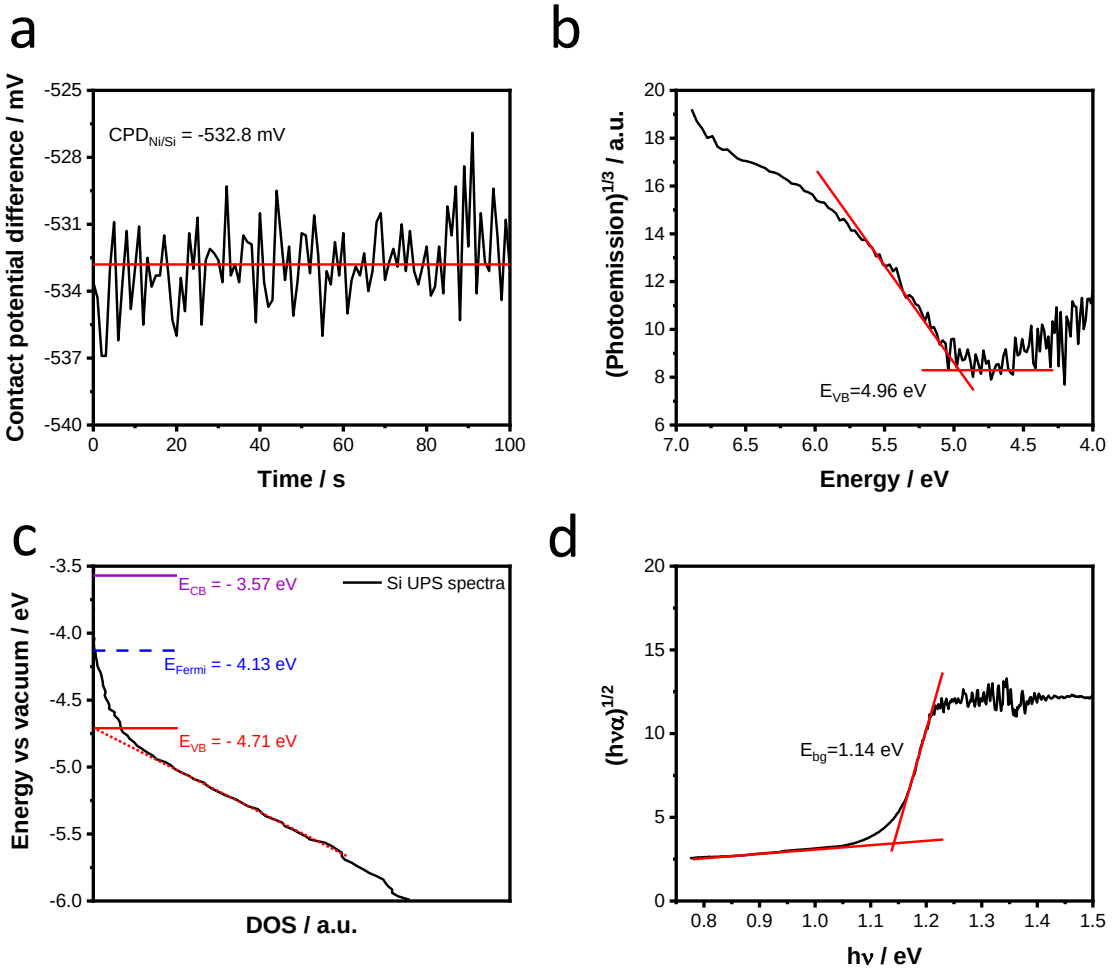

Supplementary Figure 25. Raw data from which the band energy diagram was constructed: (a) Contact potential difference measurement and (b) ambient pressure photoemission spectroscopy data. (c) Ultraviolet photoelectron spectroscopy measurement and (d) determination of bandgap energy by Tauc analysis.

XPS measurements were carried out to assess the chemical composition of the deposited Ni catalyst on the surface of the Si substrates **(Supplementary Figure 26)**. The high-resolution XPS scans of the Ni $2p_{2/3}$ region (**Supplementary Figure 26a**) reveal the presence of Ni (52 at%), $Ni(OH)_2$ (39 at%) and NiO (9 at%) on the sample surface. These results are in good agreement with the observed sharp Auger feature of Ni (**Supplementary Figure 26b**) and the different oxygen species deduced from the O 1s region (**Supplementary Figure 26c**).[5] The main $2p_{2/3}$ peak was determined to be 852.1 eV for Ni metal, 854.8 eV for $Ni(OH)_2$ and 853.7 eV for NiO respectively which agrees well with literature values.[6]

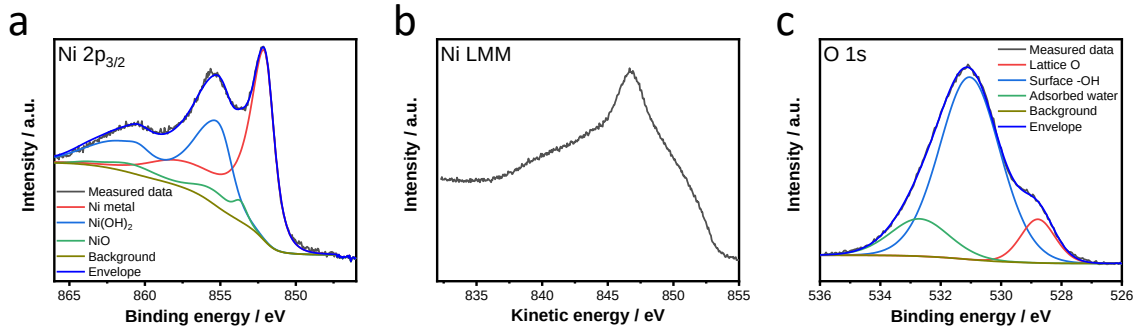

Supplementary Figure 26. XPS high resolution scans of the pristine Si/Ni samples, where (a) Ni $2p_{3/2}$, (b) Ni LMM Auger and (c) O 1s core-level region.

XPS measurements were also performed on the sample that was subjected to 8h photoelectrolysis at 1.0 V under 1 sun with HER on the cathode. We found that the surface chemical composition was altered. The Ni metal content (9 at%) of the surface was converted to hydroxide species of $Ni(OH)_2$ (45 at%) and NiOOH (46 at%) (**Supplementary Figure 27a**). This chemical composition change was reflected in the Ni Auger feature (**Supplementary Figure 27b**) and O 1s (**Supplementary Figure 27c**) spectra of the samples as well. The main $2p_{2/3}$ peak was determined to be 852.2 eV for Ni metal, 854.9 eV for $Ni(OH)_2$ and 854.7 eV for NiOOH respectively which agrees well with literature values.[6]

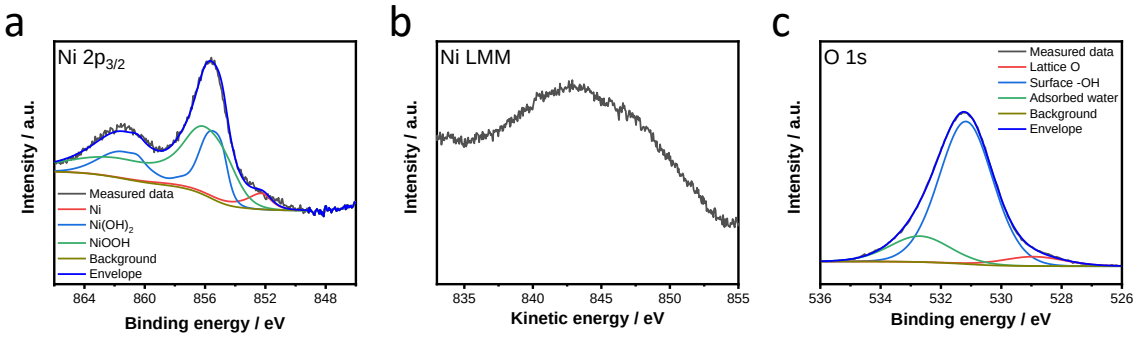

Supplementary Figure 27. XPS high resolution scans of the Si/Ni samples after 8 hours of photoelectrolysis at 1.0 V under 1 sun with HER on the cathode, where (A) Ni $2p_{3/2}$, (B) Ni LMM Auger and (C) O 1s core-level region.

Supplementary References

1. Endrődi, B. et al. High carbonate ion conductance of a robust PiperION membrane allows industrial current density and conversion in a zero-gap carbon dioxide electrolyzer cell. *Energy Environ. Sci.* **13**, 4098–4105 (2020).

2. Endrődi, B., Samu, A., Kecsenovity, E., Halmágyi, T., Sebők, D. & Janáky, C. Operando cathode activation with alkali metal cations for high current density operation of water-fed zero-gap carbon dioxide electrolysers. *Nat. Energy* **6**, 439–448 (2021).

3. Vass, Á. et al. Local Chemical Environment Governs Anode Processes in CO_2 Electrolyzers. *ACS Energy Lett.* **6**, 3801–3808 (2021).

4. Ma, M., Clark, E. L., Therkildsen, K. T., Dalsgaard, S., Chorkendorff, I. & Seger, B. Insights into the carbon balance for CO_2 electroreduction on Cu using gas diffusion electrode reactor designs. *Energy Environ. Sci.* **13**, 977–985 (2020).

5. Biesinger, M. C., Lau, L. W. M., Gerson, A. R. & Smart, R. S. C. The role of the Auger parameter in XPS studies of nickel metal, halides and oxides. *Phys. Chem. Chem. Phys.* **14**, 2434–2442 (2012).

6. Biesinger, M. C., Payne, B. P., Lau, L. W. M., Gerson, A. & Smart, R. S. C. X-ray photoelectron spectroscopic chemical state Quantification of mixed nickel metal, oxide and hydroxide systems. *Surf. Interface Anal.* **41**, 324–332 (2009).